Mathematical simulation of an end-port regenerative glass furnace

M D G M D S Carvalho, DIC, PhD
Department of Mechanical Engineering, Instituto Superio Tecnico, Portugal

F C Lockwood, BSc, DIC, PhD
Department of Mechanical Engineering, Imperial College of Science and Technology, Exhibition Road, London SW7

A mathematical model for the prediction of the performance of a glass furnace is described. It comprises sub-models for the combustion chamber, feed stock melting (batch), and the glass tank flow. The first sub-model which incorporates physical modelling for the lifted turbulent diffusion flames, soot formation and consumption, and the thermal radiation is given emphasis herein. The whole mathematical model is applied to an end-port regenerative furnace for both gas and heavy oil firing.

1 INTRODUCTION

There is currently considerable industry interest in support of the construction of a mathematical model which reliably simulates the performance of a glass melting furnace. The reasons for this interest are twofold. First, glass furnaces are large and so they are extremely costly to develop by highly empirical methods. Second, in the interests of glass purity they are most often gas-fired giving rise to the hope that straightforward and existing modelling can be used to provide an adequate description of the turbulent flow, combustion and heat transfer processes.

The vast majority of the previous glass furnace predictive studies have avoided the complexities of the combustion chamber region and confined attention to the flow in the glass tank, see (**1**) and (**2**) for example. There have been very few attempts to model a complete glass furnace. McConnell and Goodson (**3**) presented a simplified model in which global energy equations for the combustion chamber, glass melt and feed ('batch') were solved for an assumed flow and heat release, Hottel's (**4**) zone method being employed to calculate the combustion chamber radiation. Mase and Oda (**5**) effected a similar study but solved for the flow field in the glass melt assuming two-dimensionality. A further study of this kind has been performed by Novak (**6**) in which the combustion chamber flow field was more carefully estimated with the assistance of empirical data for non-reacting flows in cylindrical ducts.

A three-dimensional simulation of a glass furnace combustion chamber in which the flow field and heat release were determined from a numerical solution of the governing balance equations has been presented by Gosman *et al.* (**7**). The present study which forms the doctoral thesis of (**8**), extends the work of (**7**) to an industry furnace of differing configuration and brings into the analysis the batch and glass tank flows.

The MS was received on 30 May 1984 and was accepted for publication on 22 October 1984.

1.1 Description of the furnace

Figure 1 shows a sketch of the furnace which is of the end-port regenerative kind. Unpreheated natural gas fuel is admitted from five tube burners (see location 5 of the figure) situated in a port (3) which admits preheated air. The flame forms a loop within the combustion chamber and exits through the partner port (4). This port also contains a burner row and the furnace is alter-

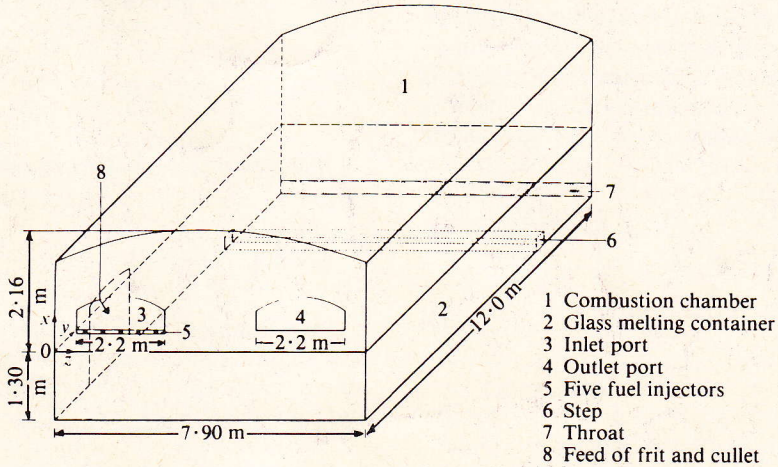

Fig. 1 Sketch of the furnace

natively fired from each port to enhance the uniformity of heat transfer to the glass surface. Since the time between port switching is relatively long the consequential transient effects are ignored and steady state calculations are performed.

The air flow is directed downwards at an angle of 16° while the fuel jets have an adjustable upward inclination, the usual value being 8°. The furnace roof and side walls are refractory lined and the roof is arched as indicated on the figure. The batch, which is a mixture of sand ('frit') and recycled glass ('cullet') enters via the port at location 8. The molten glass exits from the throat at location 7.

2 THE MATHEMATICAL SIMULATION

The present modelling problem in its entirety has three distinct parts, the simulations of the: combustion chamber, batch, and glass melt. We have treated these separately, with the aid of the same basic numerical solution procedure. The simulation of the whole furnace is a hybrid treatment involving the three codes. The modelling of the combustion chamber and the batch flow will receive particular attention here.

2.1 The combustion chamber

2.1.1 Mean flow

Time-averaged balance equations were solved in conventional fashion, see for example (**7**, **9**), for: the momenta in the x, y, z coordinate directions, the mixture fraction, f, and the specific enthalpy, h. The Favre (or density-weighted) averaged balance equations appropriate to the high Reynolds number flows all have the Cartesian tensor form:

$$\frac{\partial}{\partial x_j}(\bar{\rho}\tilde{U}_j\tilde{\phi}) = -\frac{\partial}{\partial x_j}\bar{\rho}\overline{u_j''\phi''} + \tilde{S}_\phi \tag{1}$$

where ϕ is a dependent variable: U, V, W, f and h is this case, S_ϕ is a source term, while the tildes designated density weight averages and the double primes represent instantaneous departures from these values.

2.1.2 The turbulence model

The 'standard' k–ε tubulence model was employed (**10**, **11**). In the absence of a turbulence modelling breakthrough the k–ε formulation still constitutes the best combination of economy and accuracy for engineering purposes. In density-weighted form the turbulence fluxes are:

$$\widetilde{\bar{\rho}u_i''u_j''} = \frac{2}{3}\bar{\rho}\delta_{ij}k - \mu_T\left[\frac{\partial\tilde{U}_i}{\partial x_j} + \frac{\partial\tilde{U}_j}{\partial x_i} - \frac{2}{3}\delta_{ij}\frac{\partial\tilde{U}_l}{\partial x_l}\right] \tag{2}$$

$$\widetilde{\bar{\rho}u_j''\phi''} = -\frac{\mu_T}{\sigma_T}\frac{\partial\tilde{\phi}}{\partial x_j} \tag{3}$$

where

$$\mu_T = C_\mu\bar{\rho}\frac{k^2}{\varepsilon}$$

and k and ε are obtained from solution of the transport equations:

$$\frac{\partial}{\partial x_j}(\bar{\rho}\tilde{U}_j k) = \frac{\partial}{\partial x_j}\left[\frac{\mu_T}{\partial x_j}\left(\frac{\mu_T}{\sigma_k}\frac{\partial k}{\partial x_j}\right) - \widetilde{\bar{\rho}u_i''u_j''}\frac{\partial\tilde{U}_i}{\partial x_j} - \frac{\mu_T}{\bar{\rho}^2}\frac{\partial\bar{\rho}}{\partial x_i}\frac{\partial\bar{P}}{\partial x_i}\right] - \bar{\rho}\varepsilon \tag{4}$$

$$\frac{\partial}{\partial x_j}(\bar{\rho}\tilde{U}_j\varepsilon) = \frac{\partial}{\partial x_j}\left(\frac{\mu_T}{\sigma_\varepsilon}\frac{\partial\varepsilon}{\partial x_j}\right) - C_1\frac{\varepsilon}{k}\left[\widetilde{\bar{\rho}u_i''u_j''}\frac{\partial\tilde{U}_i}{\partial x_j} - \frac{\mu_T}{\bar{\rho}^2}\frac{\partial\bar{\rho}}{\partial x_i}\frac{\partial\bar{P}}{\partial x_i}\right] - C_2\bar{\rho}\frac{\varepsilon^2}{k} \tag{5}$$

The model constants appearing in the above equations were assigned the following values, taken unchanged from Launder and Spalding (**12**); $C_\mu = 0.09$, $C_1 = 1.44$, $C_2 = 1.92$, $\sigma_k = 1.0$, $\sigma_\varepsilon = 1.3$ and $\sigma_T = 0.9$.

2.1.3 The combustion model

The fuel and air are introduced separately and burn in a turbulent diffusion flame. The usual and valid assumption is made that the rate of combustion is controlled by the mixing rate and not by the much faster chemical kinetic rate. The instantaneous gas composition, temperature and density can be determined as functions (albeit non-linear ones) of the instantaneous mixture fraction f (**7**, **9**). Since, however, f will fluctuate as any other variable in a turbulent flow, knowledge of the probability density function (PDF) of f is required if mean values of the functions of f are to be calculated. An assumed-shape PDF approach is adopted here with the PDF of f described in terms of its first two moments, namely the mean value $\tilde{f}$ and the variance $\widetilde{f''^2}$. The modelled transport equation for the latter is:

$$\frac{\partial}{\partial x_j}(\bar{\rho}\tilde{U}_j\widetilde{f''^2}) = \frac{\partial}{\partial x_j}\left(\frac{\mu_T}{\sigma_T}\frac{\partial\widetilde{f''^2}}{\partial x_j}\right) + 2\frac{\mu_T}{\sigma_T}\left(\frac{\partial\tilde{f}}{\partial x_j}\right)^2 - C_D\bar{\rho}\frac{\varepsilon}{k}\widetilde{f''^2} \tag{6}$$

The additional constant C_D in this equation was assigned the value 2.0.

A density-weighted PDF is used whose definition allows the determination of the density-weighted mean value of any quantity which is a function of f alone, thus:

$$\tilde{\phi} = \int_0^1 \phi(f)p(f)\,\mathrm{d}f \tag{7}$$

The mean gas density is obtained from the expression:

$$\bar{\rho} = \left[\int_0^1 \frac{p(f)}{\rho(f)}\,\mathrm{d}f\right]^{-1} \tag{8}$$

A β-function PDF has been utilized in the present calculations; it can be written as follows:

$$p(f) = \frac{f^{a-1}(1-f)^{b-1}}{\int_0^1 f^{a-1}(1-f)^{b-1}\,\mathrm{d}f} \qquad 0 < f < 1 \tag{9}$$

where the parameters a and b may be calculated at any point if the values of the mean and the variance are known:

$$a = \tilde{f}\,\frac{\tilde{f}(1-\tilde{f})}{\widetilde{f''^2}} - 1 \qquad b = \frac{(1-\tilde{f})}{\tilde{f}}\,a$$

The location of the onset of combustion in lifted gaseous flames may be estimated in the manner of (**13**) and (**14**).

It is presumed that no flame will be possible if the volumetric interdiffusion rate between adjacent Kolmogorov vortices exceeds the volumetric rate of chemical reaction. This situation occurs for:

$$\phi > \eta \tag{10}$$

where $\phi \equiv D/U$, D is the mass diffusion coefficient, U is the burning velocity and $\eta = 0.53(\nu^3/\varepsilon)^{1/4}$ is the Kolmogorov length scale.

The flame speed, U, will be composed of a laminar, S, and a turbulent, V, contribution. An estimate of V is obtained from the circumferential momentum equation by imagining a one-dimensional microscale vortex in solid rotation body:

$$\Delta P \sim \frac{1}{2}\,\rho_u V_\theta^2 \approx \rho_b V^2 \tag{11}$$

where, u and b designate unburnt and burnt quantities, ΔP is the pressure difference between the vortex periphery and its axis and the circumferential velocity V_θ is characterized by the Kolmogorov velocity scale:

$$V_\theta \sim (\varepsilon\nu)^{1/4} \tag{12}$$

So the estimated flame speed is:

$$U = S + C\left[\frac{1}{2}\,\frac{\rho_u}{\rho_b}\,(\varepsilon\nu)^{1/2}\right]^{1/2} \tag{13}$$

where the empirical constant C has a value of about 0.7.

The extinction criterion is then:

$$D\Big/\left\{S + C\left[\frac{1}{2}\,\frac{\rho_u}{\rho_b}\,(\varepsilon\nu)^{1/2}\right]^{1/2}\right\} > 0.53(\nu^3/\varepsilon)^{1/4} \tag{14}$$

2.1.4 The radiation model

The 'discrete transfer' radiation prediction procedure of Lockwood and Shah (**15**) has been utilized in this study. This method combines ease of use, economy and flexibility of application. This last feature is of particular importance in the real world of geometrically intricate combustion chambers. The claimed advantages of the method have now survived the rigours of several industrial applications, see (**7**) and (**16**) for example.

The 'discrete transfer' method is founded on a direct solution of the radiation transfer equation for a direction $\boldsymbol{\Omega}$ which runs:

$$\frac{\mathrm{d}I}{\mathrm{d}s} = (k_g + k_s)\left(\frac{E}{\pi} - I\right) \tag{15}$$

where I is the radiation intensity in a $\boldsymbol{\Omega}$ direction, s is distance in that direction, $E \equiv \sigma T_g^4$ is the black body emissive power, and k_g and k_s are respectively the gas and soot absorption coefficients. The scattering terms do not appear, although they are easily accommodated, since the only particulate matter occurring in the present application is the soot particles which are much too small to scatter significantly. Many radiation methods are based on the solution of the much more complex integro-differential equation which results when equation (15) is rewritten for the whole solid angle Ω. In the authors' opinion this is unsatisfactory since the numerical solution treatment of such an equation is necessarily very elaborate.

The authors prefer to solve the much simpler equation (15) within discretizations $\mathrm{d}\Omega_j$ of the whole solid angle Ω about selected directions $\boldsymbol{\Omega}$. Assuming that E, k_g and k_s are constant over a finite distance increment δs, equation (15) may be integrated to yield the simple recurrence relation:

$$I_{n+1} = \frac{E}{\pi}\,\{1 - \exp[-(k_g + k_s)\delta s]\} + I_n \exp[-(k_g + k_s)\delta s] \tag{16}$$

where n and $(n+1)$ are successive locations along $\boldsymbol{\Omega}$ separated by the increment δs. The relation is applied along the chosen $\boldsymbol{\Omega}$ from known conditions at point Q, say, (either guessed or pertaining to those of the previous iteration) on one wall to the point of impingement, P say, of the direction $\boldsymbol{\Omega}$ on an opposite wall.

If the hemisphere above P is discretized into subangles $\delta\Omega_r$, within which the intensity is considered to be uniform, the energy flux arriving at P is:

$$q_{+,P} = \int_\pi I_P \boldsymbol{\Omega}\,\mathrm{d}\Omega = \sum_{\text{all } r} I_P,\ \underset{r\to r}{\boldsymbol{\Omega}}\ \mathrm{d}\Omega_r \tag{17}$$

The wall boundary condition is:

$$q_{-,P} = (1 - \varepsilon_w)q_{+,P} + \varepsilon_w E_w \tag{18}$$

where $q_{-,P}$ is the energy leaving the wall at P, ε_w is the wall emissivity, and $E_w = \sigma T_w^4$ is the wall emissive power. The value of $I_{0,r}$ at point Q, the initial value required for the application of the recurrence relation (16), is $q_{-,P}/\pi$. The net radiation heat flux is of course:

$$q_P = q_{+,P} - q_{-,P} \tag{19}$$

The net heat gain or loss within a small control volume of the flow procedure is:

$$S_R = (I_{n+1} - I_n)\boldsymbol{\Omega}\,\mathrm{d}\Omega\,\mathrm{d}A \tag{20}$$

where the locations n and $(n+1)$ correspond to the 'entry' and 'exit' of a direction $\boldsymbol{\Omega}$ into and from a control volume, and δA is the cell wall area projected normal to $\boldsymbol{\Omega}$. The energy sources S_R are appended to the energy balance equation solved for by the flow code.

The gas absorption coefficient k_g is calculated from the 'two grey plus a clear gas' fit of Truelove (**17**). Water vapour and carbon dioxide are the prime contributors to the gaseous radiation. The total gas emittance is expressed by:

$$\varepsilon_g = \sum_n a_{g,n}(T)[1 - \exp(k_{g,n}(p_w + p_c)L] \tag{21}$$

where the summation n is over the three gases of the assumed mixture, the $k_{g,n}$ are presumed constant with the temperature dependence of the emittance being accommodated in the weighting coefficients $a_{g,n}$, p_w and p_c are the partial pressures of the water vapour and carbon dioxide and L is the path length. The values of

the $k_{g,n}$ and $a_{g,n}$ are tabulated in (**17**). The value of k_g required for these calculations is obtained from the pseudo grey approximation:

$$\varepsilon_g = 1 - \exp(-k_g L)$$

which has worked well in many furnace heat transfer computations.

2.1.5 *The soot model*

The distinctive feature of oil-fired flames is their significant soot content. The proportion of the total carbon content of the fuel which converts to soot is too small to influence significantly the overall flame heat release distribution. Rather, soot is of concern because its presence greatly augments the radiation heat transfer and because it is a pollutant. Most reasonably operated and maintained modern burners ensure complete combustion of soot. So the primary function of the soot model will be the good characterizing of the optical behaviour of the flame.

The soot content of heavy oil flames is so great that those of industrial dimensions approach the black body limit. In consequence the accurate prediction of the local soot concentration is not a prerequisite for the good calculation of the radiation transfer. This is indeed fortunate since the mechanisms of soot formation are far from being established even in the simplest laboratory flames (**18**).

A simple global expression similar to that used by Khan and Greeves (**19**) is chosen to characterize soot production:

$$P_{s+} = C_f P_{fu} \phi^n \exp(-E/T_g) \tag{22}$$

C_f is a function which ideally depends on an easily definable fuel property such as the C/H ratio. The authors have simply tuned it to flame data and have found that a value of about 0.01 is appropriate (**20**). Although the work of (**19**) was performed in connection with diesel engines we find that their values of 3 and 40200 cal/mol for n and E are useful. Soot production is essentially zero for equivalence ratios, ϕ, less than that corresponding to the incipient sooting limit (**21**) and for ϕ in excess of a value corresponding roughly to the upper flammability limit. Following Khan and Greeves the upper and lower limits have been set to 2 and 8 respectively.

In one sense the determination of the soot burning rate poses a much less demanding modelling problem since the particle sizes are so small that near-particle diffusion cannot possibly be controlling, rather the combustion rate will be controlled by, the rate of mixing of the particle-bearing vortices with adjacent oxygen bearing material. A straightforward method of estimating this rate has been proposed by Magnussen and Hjertager (**22**) who, following conventional turbulence concepts (**23**), presume that the mixing rate is proportional to the magnitude of the time mean soot concentration $\bar{m}_s$, and the time-scale of the large scale turbulence motion ε/k. Their expression for the soot consumption rate is:

$$P_{s-} = A\bar{m}_s(\varepsilon/k) \tag{23a}$$

where A is a model constant assigned the value 4 based on numerical experimentation. This relation will not be satisfactory in regions where the reaction rate is limited by oxygen deficiency in which case Magnussen and Hjertager propose:

$$P_{s-} = A\left(\frac{\bar{m}_{ox}}{\bar{m}_s S_s + \bar{m}_{fu} S_{fu}}\right)\bar{m}_s\left(\frac{\varepsilon}{k}\right) \tag{23b}$$

where the S_s and S_{fu} are the soot and fuel stoichiometric ratios. The alternative giving the smallest reaction rate is to be used.

2.2 The batch model

The batch or feed problem is sketched in Fig. 2. The width of the batch flow is small relative to its length, and the predominant flow direction is in the sense of the longer dimension. The (laminar) boundary layer equations may therefore be utilized of the form:

$$\frac{\partial}{\partial z}(\rho w\phi) + \frac{\partial}{\partial y}(\rho v\phi) = \frac{\partial}{\partial y}\left(\Gamma_\phi \frac{\partial \phi}{\partial y}\right) + S_\phi \tag{24}$$

The solution domain lies within the region contained by the boundaries designed I and E on the figure. Due to a shortage of time variations in the direction normal to the page have been neglected. No matter of principle precludes the performance of fully three-dimensional calculations, but cross-stream effects are unlikely to be large.

In the spirit of the boundary layer approximations dynamic pressure variations in the vertical direction have been neglected. The newly formed glass on the surface of the batch is permitted to run off under the influence of gravity. The property values for the frit and the glass were taken from (**24**). In addition to that for mass conservation equations of the form (24) were

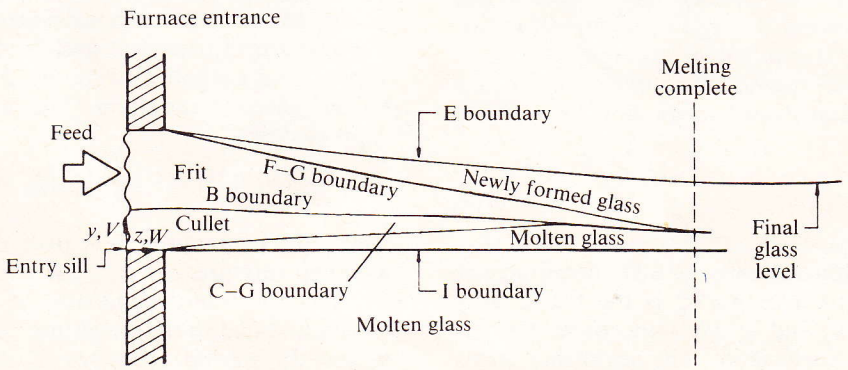

Fig. 2 Geometry of the batch flow

solved across the whole of the batch for the streamwise momentum and for energy conservation.

The hydrostatic pressure gradient source term appears in the streamwise momentum equation:

$$\frac{dp}{dz} = -g\rho \frac{dn}{dz} - \frac{d}{dz}\int_n^y a_y \, \Delta\rho \, dy \qquad (25)$$

where n is the level of the I boundary, and a_y is the cross-stream component of the gravitational acceleration g.

The absorption of radiation within the thin melted glass regions of the batch was ignored, the incident heat flux from the combustion chamber being introduced at the surface of the unmelted cullet. The solid body motion of the unmelted frit and cullet was assured by the imposition of a large viscosity value.

2.3 The glass tank

The calculations of the buoyancy dominated glass melt is a fairly straightforward undertaking by modern computational techniques. The continuity, momenta and energy balance equations have been solved in three dimensions for industry specified boundary conditions. The property values are again as specified in (**24**). The radiation transfer was handled by the Rosseland (optically thick) approximation which results in appropriately augmented thermal conductivities in the energy balance equation. The side walls of the furnace were allowed to lose heat to the surroundings at a rate dictated by an estimated overall heat transfer coefficient. The bottom of the furnace was presumed to be adiabatic. The heat transfer to the top surface of the melt was that calculated for the combustion chamber.

3 SOME COMPUTATIONAL INFORMATION

3.1 The combustor chamber

The effect of grid refinement was explored using three grids of: $7 \times 9 \times 8$, $8 \times 13 \times 12$ and $9 \times 16 \times 17$ nodes. On the basis of this fourfold increase in the number of grid nodes it is estimated that the last mentioned resulted in predicted values differing from the numerically exact ones by less than 10 per cent. At this stage the improved accuracy of a finer grid did not justify the additional expense. The mildly arched roof was accommodated with small error within the orthogonal mathematical framework by: (*i*) suitable adjustments to the area coefficients of the finite-difference equations, and (*ii*) the appending of extra terms to these equations to account for the extra mass fluxes entering a finite-difference cell consequent of the inclination of the cell wall with respect to the coordinate direction.

The row of individual gas burners was simulated by a slot. The real burner inlet velocities and momenta were always maintained. Normally the fuel jets were inclined upwards while the incoming air stream was usually directed slightly downwards. For the case of oil firing the spray is supposed to evaporate instantaneously in the grid cell adjacent to the plane of the atomizers. The presence of the spray was made known to the governing equations for the gas phase through appropriate source terms. This is a major simplification which is justified only when the near burner field is not of primary interest. A more elaborate simulation would track droplet flights but the added computational expense could not be justified at this stage.

Boundary condition information has been stored two-, rather than three-, dimensionally for economy purposes. The finite-difference equations are solved by alternating direction line iteration in the x–y planes. Because of the loosely parabolic nature of the flow, away from the entry port and towards the exit port, a considerable economic advantage accrued from the use of a plane by plane solution approach with the 'sweeps' being conducted in the z-direction. Because of the elliptic behaviour of pressure, it was found necessary to compute and store the coefficients of the pressure correction finite-difference equation three-dimensionally.

3.2 The batch calculation

The basic TEACH code was modified to handle the parabolic batch calculations. The streamwise diffusional terms were excluded and a marching integration scheme was introduced. The grid was caused to contract with the I and E boundaries (Fig. 2) by numerical modifications analogous to the above-mentioned ones for the arched roof of the combustion chamber. The cross-stream grid contained forty nodes.

Iteration was employed between adjacent upstream and downstream stations to ensure conservation. The procedure may be summarized as follows: (*i*) the w-momentum (streamwise) momentum equation was solved at the downstream location using known upstream information, (*ii*) the v-velocity (cross-stream) was determined from continuity, (*iii*) the energy balance equation was solved, and the amount of newly melted material determined, (*iv*) the grid contraction was calculated to satisfy mass continuity, (*v*) the values of the downstream station physical properties were updated, (*vi*) the sequence was repeated from (*i*) until convergence was achieved.

4 A FEW RESULTS

4.1 The combustion chamber

Runs for methane fuel both with and without nitrogen dilution and for heavy oil firing have been performed. Additionally, the excess air level and the inlet port area were varied. The fuel energy input was 30 MW in all cases. Space limitations permit only a small fraction of the information generated by the runs to be reported. The industry orientated reader will find full information in (**8**). Some typical detailed predicted information is portrayed in Figs. 3a–3c which show respectively for heavy oil firing: contours of fuel concentration within the combustion chamber, the refractory roof temperature contours, and the net heat flux contours at the surface of the glass melt.

The diluted methane fuel contained 14 per cent nitrogen to simulate Dutch natural gas. In summary the dilution as expected reduces somewhat the total heat transfer and the temperature of the refractory roof compared with the undiluted fuel case. Interestingly, because dilution shortens a turbulent flame the non-uniformity of the heat flux to the melt is increased. Similarly, increasing the excess air not only lowers the total heat

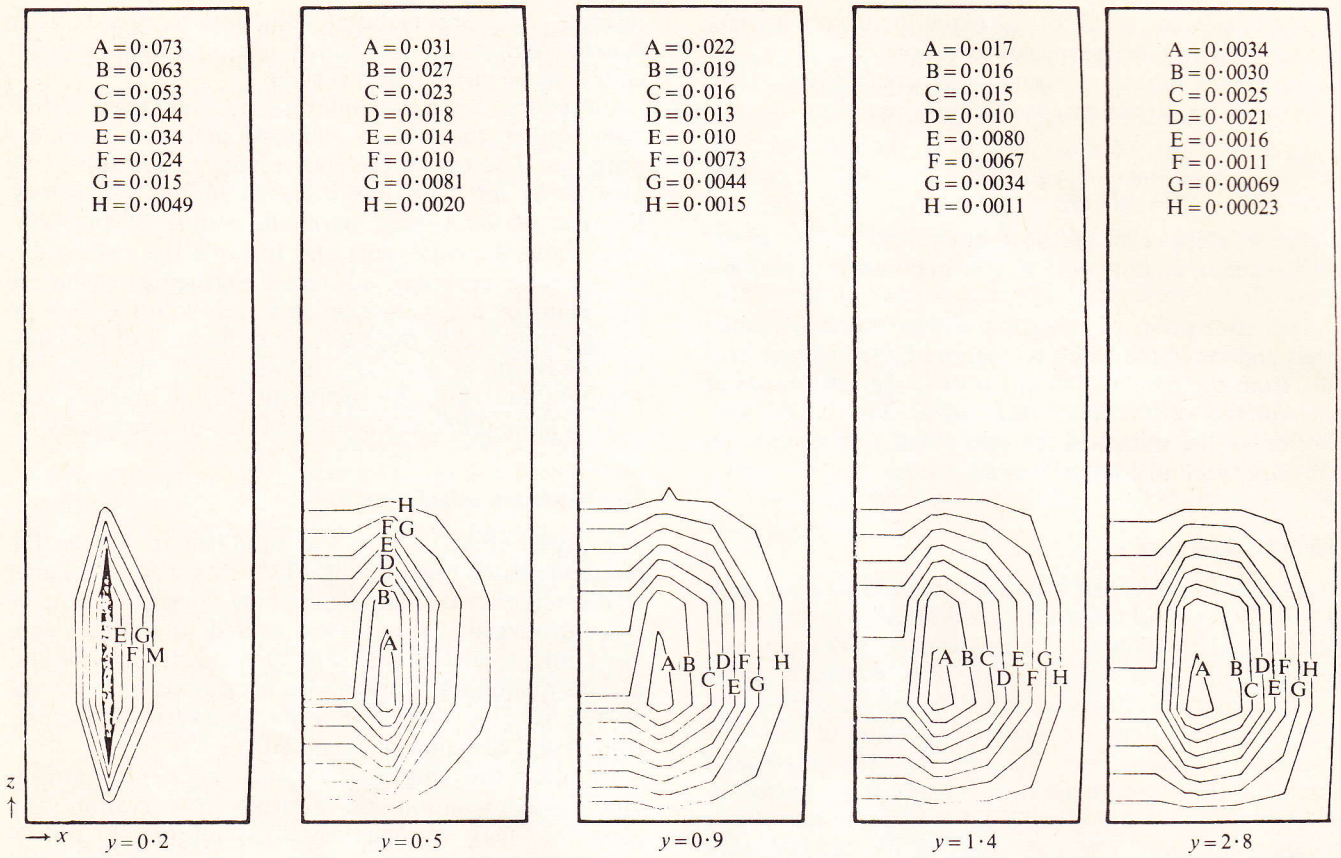

(a) Contours of fuel mass fraction

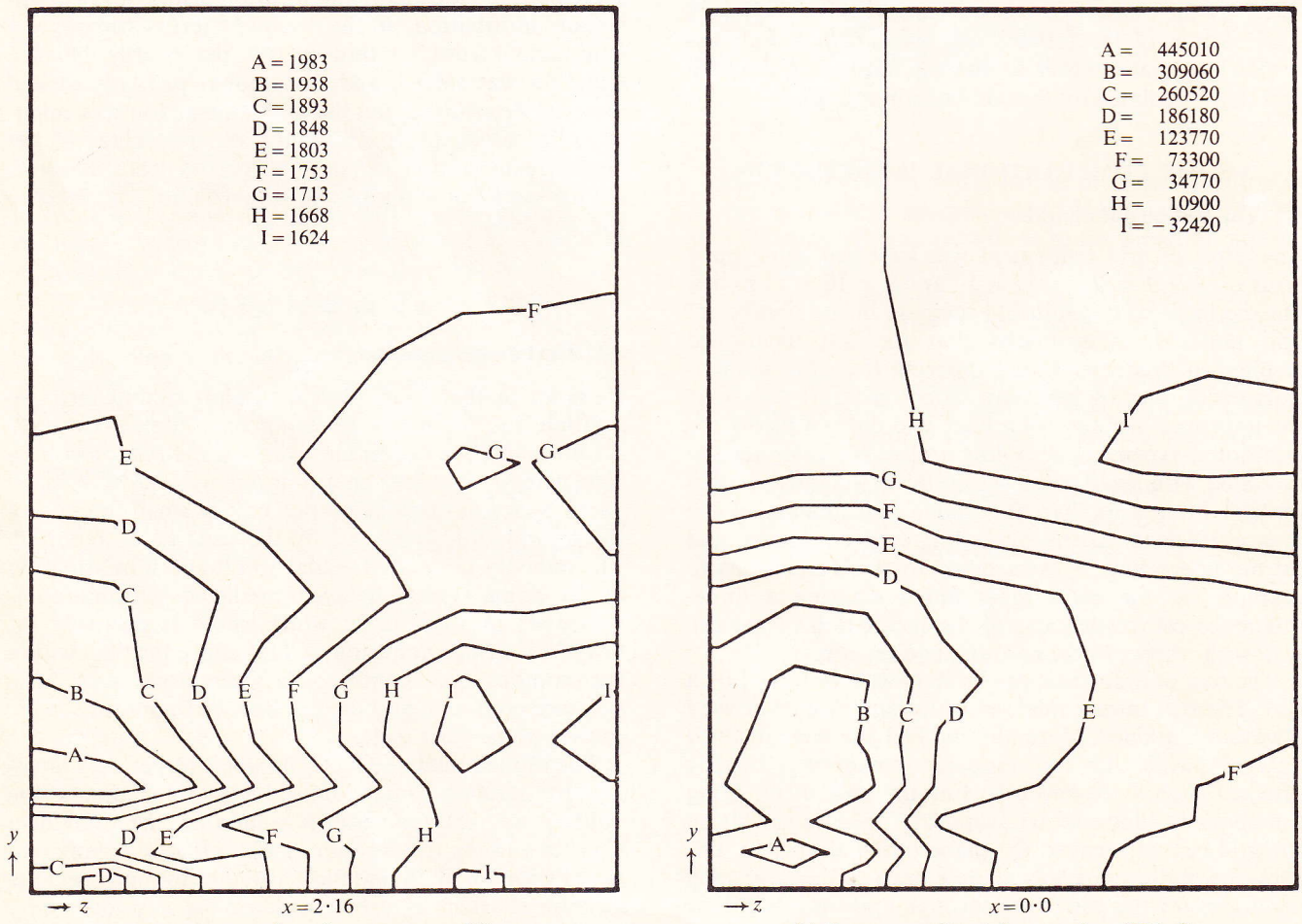

(b) Contours of roof temperature (K)

(c) Contours of heat flux to glass (W/m^2)

Fig. 3 Some predictions for heavy oil firing (see Fig. 1 for coordinates)

Table 1 Comparison between oil-fired and natural gas-fired furnace performance

	Natural gas	Heavy oil
Total radiation to glass, W	1.071×10^7	1.124×10^7
Total convection to glass, W	1.80×10^5	8.08×10^4
Outlet temperature, K	1678	1650
Maximum roof temperature, K	1830	1983
Outlet velocity, m/s	16.1	15.8

transfer and chamber temperatures, but increases the non-uniformity of the glass melt surface heat flux. Reducing the air inlet port area also worsens the heat flux non-uniformity as a consequence of flame shortening. In general, however, the performance of this furnace displays a notable resistance to alterations in the input variables and this fact more than any other is not doubt responsible for its widespread use over many years.

Table 1 compares some key performance criteria for heavy oil and natural gas firing, the firing rates being 30 MW with 8 per cent excess air in both cases. As expected the useful heat transfer is greater for oil firing, but by only some 5 per cent since the radiative path lengths are large enough for the gaseous emissivity to be near the optically thick limit. The heat transfer peak in the near burner region is more pronounced for oil firing than for gas firing; this fact is reflected in the maximum roof temperatures cited in Table 1.

The necessity of adhering to the production schedule and the hostile environment of a real glass furnace make the obtaining of good data an extremely difficult task. Exhaust gas exit temperatures may, however, be fairly well determined. The value of 1678 K of Table 1 for gas firing is to be compared with the industry measured one of 1700 K.

4.2 The batch flow

The effect of batch: preheating, layer thickness, mass flowrate and composition (cullet/frit ratio) have been investigated in twelve separate runs. The four runs in which the amount of preheat was varied are presented as a sample of these parametric studies in Table 2. Figure 4 depicts the evolution of the batch flow for case 1. Again, full details of all the runs are available in (**8**).

5 CONCLUDING REMARKS

This paper has demonstrated that the present day computation procedure can be applied to predict the entire fluid flow behaviour of an industrial glass furnace. Because of the experimental difficulties and cost very few data exist against which the predictions can be validated, but the predictions are supported by what few data do exist and also, the authors should stress, in a general way by the operating experience of the industry concerned. The authors would very much like to have identified changes in operating conditions likely to lead to enhanced performance of the present furnace. Instead, and somewhat surprisingly, it was found that

Table 2 Effect of batch preheat on batch melt length and surface temperature

Case	Y_E m	Inlet velocity m/s	Mass inflow rate kg/s	Cullet/batch mass ratio	T_{inlet} K	Melt length m	Batch surface temperature
1	0.2	0.00063	0.1912	0.3	623	3.84	Identical temp. profile
2	0.2	0.00063	0.1912	0.3	288	4.90	curves result, shifted
3	0.2	0.00063	0.1912	0.3	373	4.62	by the difference
4	0.2	0.00063	0.1912	0.3	473	4.14	in preheat temp.

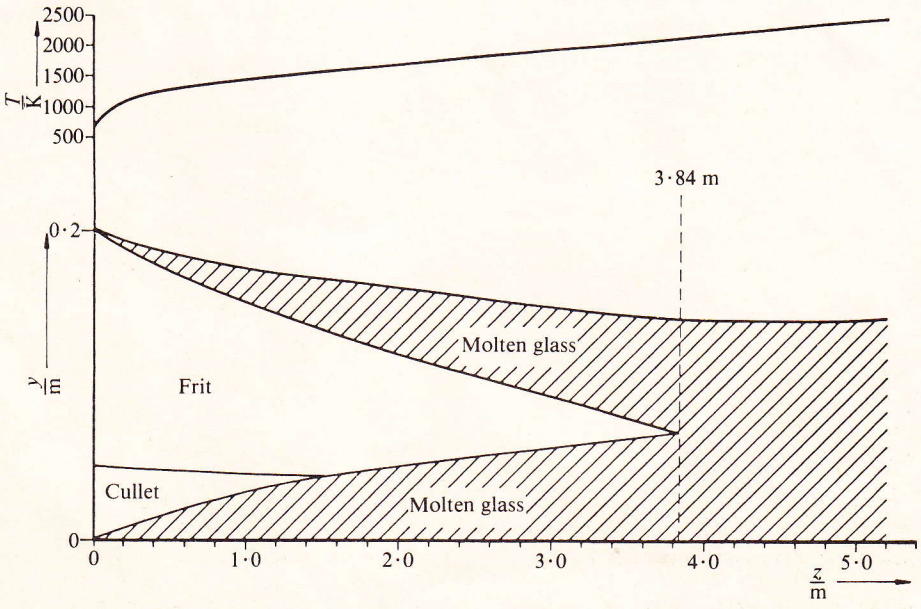

Fig. 4 Evolution of the batch melt and top surface temperature. Case 1, see Table 2

its performance is fairly insensitive to normally experienced changes in operating conditions and minor design alterations. This robustness is no doubt the reason for this furnace's longevity in the glass producing industry.

REFERENCES

1 **Chen, T.** and **Goodson, R. E.** Computation of three-dimensional temperature and convective flow profiles for an electric glass furnace. *Glass Tech.*, 1972, **13**(6), 161–167.

2 **Suzuki, J.** Three-dimensional flow and temperature distributions in rectangular cavities. MSc Thesis, University of Sheffield, 1976.

3 **McConnell, R. R.** and **Goodson, R. E.** Modelling of glass furnace design for improved energy efficiency. *Glass Tech.*, 1979, **20**(3).

4 **Hottel, H. C.** and **Sarofim, A. F.** *Radiative transfer*, 1967 (McGraw-Hill, New York).

5 **Mase, H.** and **Oda, K.** Mathematical model of glass tank furnace with batch melting process. *J. Non-Crystalline Solids*, 1980, **38** and **39**, 807–812.

6 **Novak, J. D.** Application of combustion space energy calculations to commercial glass furnaces. *J. Non-Crystalline Solids*, 1980, **38** and **39**, 819–824.

7 **Gosman, A. D., Lockwood, F. C., Megahed, I. E. A.** and **Shah, N. G.** The prediction of the flow, reaction and heat transfer in the combustion chamber of a glass furnace. AIAA 18th Aerospace Sciences Meeting, California, 1980.

8 **Carvalho, M. D. G. M. D. S.** Computer simulation of a glass furnace. PhD thesis, London University, 1983.

9 **Abou Ellail, M. M. M., Gosman, A. D., Lockwood, F. C.** and **Megahed, I. E. A.** Description and validation of a three-dimensional procedure for combustion chamber flows. *J. Energy, AIAA*, April 1978. Also *Progress in Astronautics and Aeronautics, Turbulent Combustion*, Vol. 58, 1977. Editor: Lawrence A. Kennedy (AIAA).

10 **Launder, B. E., Morse, A. P., Rodi, W.** and **Spalding, D. B.** The prediction of free shear flows—a comparison of the performance of six turbulence models. Proceedings NASA Conf. on Free Shear Flows, Langley, 1972.

11 **Jones, W. P.** and **Launder, B. E.** Predictions of low Reynolds number phenomena with a two-equation model of turbulence. *Int. J. Heat Mass Transfer*, 1973, **16**, 119.

12 **Launder, B. E.** and **Spalding, D. B.** The numerical computation of turbulent flows. *Comput. Meth. App. Mech. and Engng*, 1973, **3**.

13 **Lockwood, F. C.** and **Megahed, I. E. A.** Extinction in turbulent reacting flows. *Combustion Science and Technology*, 1978, **19**, 77–80.

14 **Chakravarty, A., Lockwood, F. C.** and **Sinicropi, G.** The prediction of burner stability limits for lower calorific gas fuels. Submitted Mech. Engng. Dept., Imperial College, Fluids Section Report FS/83/40, 1983.

15 **Lockwood, F. C.** and **Shah, N. G.** A new radiation solution method for incorporation in general combustion prediction procedures. 18th Symposium (International) on Combustion, The Combustion Institute, 1980.

16 **Lockwood, F. C., McGuirk, J. J.** and **Shah, N. G.** Radiation transfer in gas turbine combustors. Presented at AIAA 18th Thermophysics Conference, Paper No. AIAA-83-1506, June, 1983.

17 **Truelove, J. S.** A mixed grey gas model for flame radiation. AERE Harwell Report No. HL76/3448/KE.

18 **Wagner, H. G. G.** Soot formation in combustion. 17th Symposium (International) on Combustion, The Combustion Institute, 1978.

19 **Khan, I. M.** and **Greeves, G.** A method for calculating the formation and combustion of soot in diesel engines. *Heat Transfer in Flames*, Ed. Afgan and Beer, 1974, pp 391–402.

20 **Abbas, A. S., Koussa, S. S.** and **Lockwood, F. C.** The prediction of a variety of heavy oil flames. Proceedings of ASME Winter Annual Meeting, Special Session on Two Phase Combustion Liquid Fuels, Washington, Nov. 1981.

21 **Glassman, I.** and **Yaccarino, P.** The temperature effect in sooting diffusion flames. Proceedings of 18th Symposium (International) on Combustion, The Combustion Institute, 1981.

22 **Magnussen, B. F.** and **Hjertager, B. H.** On mathematical modelling of turbulent combustion with special emphasis on soot formation and combustion. 16th Symposium (International) on Combustion, The Combustion Institute, 1976.

23 **Tennekes, H.** and **Lumley, J. L.** *A first course in turbulence*, 1973 (The MIT Press, Cambridge, Ma.).

24 *Batch-melting model*, Research and Development Labs., Lathom, Science Group, Pilkington Bros., 1970.